Smart Materials and Structures

PAPER

Modeling of a partially debonded piezoelectric actuator in smart composite laminates

To cite this article: Bin Huang *et al* 2015 *Smart Mater. Struct.* **24** 075013

View the article online for updates and enhancements.

You may also like

- A particle debonding model considering interface nanoscale damage effect
Yu Liu, Jieshi Chen and Xianghuai Dong
- Investigation of the interface between $LiNbO_3$ and Si fabricated via room-temperature bonding method using activated Si nano layer
Seigo Murakami, Kaname Watanabe and Ryo Takigawa
- Debonding quantification in adhesive bonded joints by the inverse finite element method
Dario Poloni, Daniele Oboe, Claudio Sbarufatti et al.

This content was downloaded from IP address 166.104.17.164 on 20/11/2023 at 02:18

IOP Publishing Smart Materials and Structures
Smart Mater. Struct. 24 (2015) 075013 (12pp) doi:10.1088/0964-1726/24/7/075013

Modeling of a partially debonded piezoelectric actuator in smart composite laminates

Bin Huang[1,2], Heung Soo Kim[2] and Gil Ho Yoon[3]

[1] Piezoelectric Device Laboratory, School of Mechanical Engineering & Mechanics, Ningbo University, Ningbo, Zhejiang 315211, People's Republic of China
[2] Department of Mechanical, Robotics and Energy Engineering, Dongguk University-Seoul, 30 Pildong-ro 1-gil, Jung-gu, Seoul 100-715, Korea
[3] Department of Mechanical Engineering, Hanyang University, Seoul, Korea

E-mail: heungsoo@dgu.edu

Received 26 January 2015, revised 28 April 2015
Accepted for publication 28 April 2015
Published 4 June 2015

Abstract

A partially debonded piezoelectric actuator in smart composite laminates was modeled using an improved layerwise displacement field and Heaviside unit step functions. The finite element method with four node plate element and the extended Hamilton principle were used to derive the governing equation. The effects of actuator debonding on the smart composite laminate were investigated in both the frequency and time domains. The frequency and transient responses were obtained using the mode superposition method and the Newmark time integration algorithm, respectively. Two partial actuator debonding cases were studied to investigate the debonding effects on the actuation capability of the piezoelectric actuator. The effect of actuator debonding on the natural frequencies was subtler, but severe reductions of the actuation ability were observed in both the frequency and time responses, especially in the edge debonded actuator case. The results provided confirmation that the proposed modeling could be used in virtual experiments of actuator failure in smart composite laminates.

Keywords: actuator debonding, failure, actuation ability, improved layerwise theory, finite element method, dynamic characteristics

(Some figures may appear in colour only in the online journal)

1. Introduction

Composite laminates with active piezoelectric layers or distributed piezoelectric actuators and sensors have been comprehensively studied in the past few decades. With their active piezoelectric elements, these structures are considered as smart [1] or adaptive composite ones [2] which have the capability of actuation and sensing. They can be used in the active vibration control [3] and energy harvesting [4, 5] industries. The piezoelectric materials are usually bonded on the surface or embedded in the host structures. In most previous studies, many theories [6, 7] were developed based on the mathematical modeling of smart composite structures with the assumption that the piezoelectric layers are perfectly bonded. However, actuator failures, such as cracks or debonding, may occur during the service life of the structures. For example, interlaminar peeling stresses [8] exist at the piezoelectric layer interface that could lead to the debonding of the piezoelectric layers. As a result of such debonding, not only the strength of the structure is weakened, but also the actuation and sensing ability of the piezoelectric elements are decreased. Additionally, the dynamic behaviors [9, 10] are also changed due to the effect of debonding.

Until now, a large number of studies [11, 12] have introduced the modeling of smart composite laminates with or without damage, such as delamination, debonding and cracks. In these modeling methods, one of the ways of dealing with the damage is by applying specific continuity conditions or constraints at the debonded regions. Seeley and Chattopadhyay [13, 14] developed a refined higher order theory based formulation for composite laminates with debonded piezoelectric actuators and sensors. The continuity conditions at the interface of the non-debonded and debonded regions

 © 2015 IOP Publishing Ltd Printed in the UK

were formulated and implemented using a penalty approach in the finite element model. Their results were subsequently verified by experiment [15]. Nanda and Sahu [16] developed a model of delamination using a first order shear deformation theory based finite element method by forcing the multipoint constraint algorithm for the delamination. They investigated the effect of the delamination size on the free vibration. Another way of modeling the delamination in composite laminates is by using the Heaviside unit step function. Kim *et al* [17–20] developed theories using the Heaviside functions to address the discontinuity of the displacement field in smart composite laminates. They investigated the delamination effect on the dynamic characteristics of smart composite structures. Oh *et al* [21] and Kim [22] developed a higher-order zigzag theory based delamination modeling using the Heaviside unit step function. The smooth transition of the displacement in the thickness direction with a Fermi–Dirac distribution function was developed for the delamination modeling by Kim *et al* [23–25].

Sun *et al* [26] investigated the effect of actuator and sensor debonding on the vibration control of beam structures. They found that the debonding decreases the control efficiency of vibration suppression. Kumar *et al* [27] also investigated the vibration control of plates with partially debonded piezoelectric actuators. The reduced stiffness was taken as an input in their controller design. The presence of debonding in active structures reduces not only their load carrying ability, but also their control ability. Moreover, it may lead to instability in the closed loop control system. Given all of these potential problems, the detection of actuator debonding is quite important in active structures.

In this work, we present a new mathematical modeling to evaluate the dynamic behaviors of smart composite laminates with partially debonded piezoelectric actuators. We use the improved layerwise theory for the displacement assumption and the Heaviside unit step function for the modeling of the partially debonded piezoelectric actuator. For the numerical solutions, the finite element procedure is implemented taking into consideration of the electro-mechanical coupling effect. Using the obtained governing equation, the dynamic responses of the partially debonded piezoelectric actuators in smart composite laminates are solved. To better understand the debonding effect on the dynamic behaviors, both the frequency response and transient response are investigated.

2. Modeling of debonded smart composite laminates

2.1. Modeling descriptions

In this subsection, the mathematical modeling of a smart composite laminate with partially debonded piezoelectric actuator is introduced. For the geometric configuration given in figure 1, one piezoelectric actuator and one piezoelectric sensor are attached to the surface of the clamped laminated composite plate. The rectangular actuator is bonded 1 cm away from the clamped root with dimensions of $5\times4\times0.2$ cm. The sensor is bonded 7 cm away from the clamped root with dimensions of $2\times2\times0.2$ cm. The clamped plate has dimensions of $30\times6\times0.2$ cm and consists of a sequence of orthotropic composite layers with various fiber orientations. The actuator is assumed to be partially debonded, which can be seen from the lateral view in figure 1. Thus, to build the mathematical model of these kinds of laminated composite structures with debonding, finite element method based formulations can be derived based on the improved layerwise theory [13, 24].

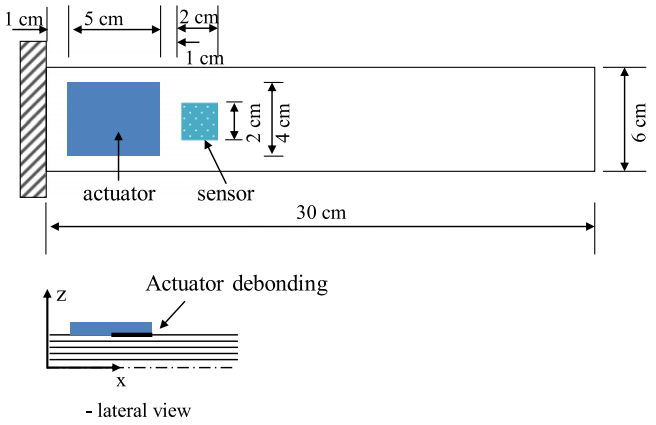

Figure 1. Geometric configuration of smart composite laminate with partially debonded piezoelectric actuator.

The constitutive relations of piezoelectric materials considering the electromechanical coupling effect are linear if they are under small electric fields and small structural displacements. These relations can be expressed as follows

$$\begin{aligned}\{D\} &= [d]^T\{\varepsilon\} + [b]\{E\}\ \text{(converse effect)},\\ \{\sigma\} &= \ [Q]\{\varepsilon\} - [d]\{E\}\ \text{(direct effect)},\end{aligned} \tag{1}$$

where $\{D\}$ is the electric displacement vector and $\{\varepsilon\}$, $\{\sigma\}$ and $[Q]$ are the strain vector, stress vector and elastic stiffness matrix, respectively. The piezoelectric constant matrix and permittivity matrix are denoted by $[d]$ and $[b]$, respectively. The electric field vector is denoted by $\{E\}$.

The extended Hamilton principle is used to derive the governing equations for an elastic system with piezoelectric elements

$$\delta\int_{t_1}^{t}(T-U+W)\mathrm{d}t = 0, \tag{2}$$

where t_1 and t are the initial and final times, respectively, T is the kinetic energy, U is the potential energy (strain energy and electrical potential energy) and W is the external work done by the traction force f and the applied surface charge q_e. These energy terms are defined as

$$\begin{aligned}T &= \int_V \frac{1}{2}\rho\{\dot{u}_i\}^T\{\dot{u}_i\}\mathrm{d}V,\\ U &= \int_V \frac{1}{2}\{\sigma\}^T\{\varepsilon\}\mathrm{d}V + \int_V \frac{1}{2}\{D\}^T\{E\}\mathrm{d}V,\\ W &= \int_S \{f_i\}^T\{u_i\}\mathrm{d}S + \int_S q_e\phi\mathrm{d}S,\end{aligned} \tag{3}$$

where the subscript V denotes the volume domain, S denotes the surface domain, u is the displacement, ρ is the mass density and ϕ is the electric potential. The traction force and

applied electric charge on the surface are denoted by f_i and q_e, respectively.

The kinematics of the smart composite laminate is modeled by using the improved layerwise theory [17]. The assumed displacement functions are shown in the following equations

$$\begin{aligned} U_i^k(x, y, z, t) &= u_i + A_i^k(z)\phi_1 + B_i^k(z)\phi_2 \\ &+ C_i^k(z)w_{,x} + D_i^k(z)w_{,y} + \overline{E}_i^j(z)\overline{w}_{,x}^j \\ &+ \overline{F}_i^j(z)\overline{w}_{,y}^j + \sum_{j=1}^{N-1}\overline{u}_i^j H(z - z_j), \\ U_3^k(x, y, z, t) &= w(x, y, t) + \sum_{j=1}^{N-1}\overline{w}^j(x, y, t)H(z - z_j), \end{aligned} \tag{4}$$

where subscript i denotes the coordinates with respect to x or y and k denotes the kth layer of the laminate. The quantities U_i^k denote the in-plane displacements and U_3^k denotes the transverse deflection. The quantities u_i and w denote the displacements of each reference plane, and ϕ_1 and ϕ_2 are the rotations of the normal to the reference plane. The multipliers $\overline{u}_i^j$ and $\overline{w}^j$ are the coefficients of the Heaviside step function H that accounts for the sliding of the in-plane displacements and possible jump of the out-of-plane displacement, respectively. The delaminated interface is denoted by z_j. The layerwise coefficients A_i^k, B_i^k, C_i^k, D_i^k, $\overline{E}_i^j$ and $\overline{F}_i^j$ are expressed in terms of the geometric and material properties [28]. To simulate the debonding effect, the coefficients of the Heaviside unit step function are nonzero, while, for the perfectly bonded interface, the coefficients are set to zero.

For the assumed displacement field, it satisfies the in-plane displacement continuity condition at the layer interfaces for both the perfectly bonded and debonded interfaces

$$\begin{aligned} &U_i^k(z_{k+1}) = U_i^{k+1}(z_{k+1}), \\ &(k = 1,\ldots, N-1, \quad i = 1, 2). \end{aligned} \tag{5}$$

The kinematic relation for the elastic strain is further obtained using the strain–displacement relation. It is to be noted that the normal strain ε_{33}^k is zero, due to the assumption that the out-of-plane displacement is independent of the z axis

$$\varepsilon_{ij}^k = \frac{1}{2}\left(U_{i,j}^k + U_{j,i}^k\right), \quad (i, j = 1, 2, 3). \tag{6}$$

The transverse shear stresses also satisfy the continuity condition at the layer interfaces, while, at the debonded interface, they are still continuous by setting the transverse shear stresses to zero

$$\begin{aligned} &\sigma_{i3}^k(z_{k+1}) = \sigma_{i3}^{k+1}(z_{k+1}), \\ &(i = 1, 2, \quad k = 1,\ldots, N-1). \end{aligned} \tag{7}$$

The electric potential function ϕ^j for the jth layer is assumed to vary according to a cubic function in the piezoelectric layer in the thickness direction, while it is zero for the other layers. A cubic distribution of the electric potential field can satisfy the surface boundary conditions of applied voltages and charge conservation law

$$\begin{aligned} \phi^j(x, y, z, t) &= \phi_0^j(x, y, t) - \left(z - z_0^j\right)E_z^j(x, y, t) \\ &+ 4\left(\frac{z - z_0^j}{h^j}\right)^2 \times \left[\left(z - z_0^j\right)\left(\frac{\overline{\phi}^j(x, y, t)}{h^j} + E_z^j(x, y, t)\right)\right. \\ &\left. - \phi_0^j(x, y, t)\right], \end{aligned} \tag{8}$$

where ϕ_0^j and E_z^j are the mid-plane electric potential and the electric field of the jth piezoelectric layer, respectively. The term $-(z - z_0^j)E_z^j$ is used to address the linear electric potential distribution in the thickness direction. The higher order term is used to address the nonuniform electric potential distribution in the thickness direction, while satisfying the equipotential electrical boundary conditions prescribed on the electrodes. The quantity $\overline{\phi}^j$ denotes the potential difference on the top and bottom electrodes in the jth piezoelectric transducer. The mid-plane position and thickness of the jth piezoelectric layer are denoted by z_0^j and h^j, respectively.

The electric field $\{E\}$ is correlated with the electric potential ϕ by differentiating the scalar potential function, as shown in equation (9)

$$\{E\} = -\left\{\frac{\partial\phi}{\partial x} \quad \frac{\partial\phi}{\partial y} \quad \frac{\partial\phi}{\partial z}\right\}^T. \tag{9}$$

2.2. Finite element formulation

The finite element method can deal with the structures of complicated geometries as well as various boundary conditions. For such kind of laminated plate structures with piezoelectric patches, we prefer using a four-node plate element for the vibration analysis. It should be noted that from the displacement field and electric potential field, it has eight structural unknowns $\left(u_1, u_2, \phi_1, \phi_2, \overline{u}_1^j, \overline{u}_2^j, w, \overline{w}^j\right)$ and two electrical unknowns (ϕ_0^j, E_z^j). To implement the finite element method, the linear Lagrange function is adopted to interpolate the in-plane structural unknowns $\left(u_1, u_2, \phi_1, \phi_2, \overline{u}_1^j, \overline{u}_2^j\right)$ and electrical unknowns $\left(\phi_0^j, E_z^j\right)$, while for the out-of-plane structural unknowns $\left(w, \overline{w}^j\right)$, the Hermite cubic interpolation function is preferred. These structural and electrical unknowns can be expressed in terms of nodal values and interpolation functions, as follows:

$$\begin{aligned} \left(u_1, u_2, \phi_1, \phi_2, \overline{u}_1^j, \overline{u}_2^j\right) &= \sum_{m=1}^{n} N_m\left[(u_1)_m, (u_2)_m, \left(\phi_1\right)_m,\right. \\ &\left.\times\left(\phi_2\right)_m, \left(\overline{u}_1^j\right)_m, \left(\overline{u}_2^j\right)_m\right], \\ \left(\phi_0^j, E_z^j\right) &= \sum_{m=1}^{n}\left[N_m\left(\phi_0^j\right)_m, N_m\left(E_z^j\right)_m\right], \end{aligned}$$

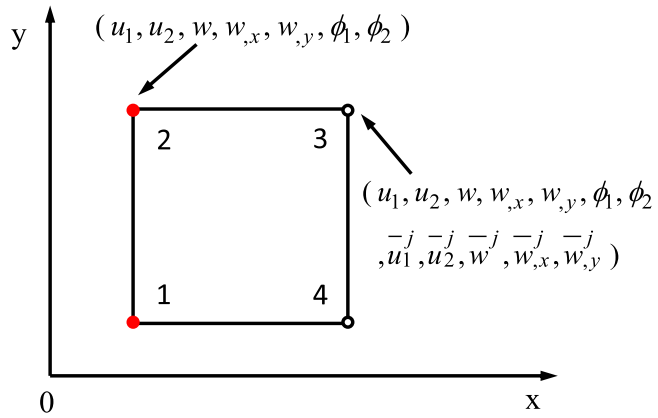

Figure 2. Four-node plate element with DOFs, node 1, 2: healthy nodes; node 3, 4: debonded nodes.

$$w = \sum_{m=1}^{n}\left[H_m(w)_m + H_{xm}(w_{,x})_m + H_{ym}(w_{,y})_m\right],$$
$$\overline{w}^j = \sum_{m=1}^{n}\left[H_m(\overline{w})_m + H_{xm}\left(\overline{w}_{,x}\right)_m + H_{ym}\left(\overline{w}_{,y}\right)_m\right], \quad (10)$$

where N_m is the Lagrange interpolation function, H_m, H_{xm} and H_{ym} are Hermite interpolation functions, and n is the number of nodes in one element.

Equation (10) can be rewritten in the matrix form and expressed by the following equation. For the four-node plate element, the DOFs for healthy nodes and debonded nodes are shown in figure 2

$$\left\{u_u^e\right\} = \left[N_u\right]\left\{d_u\right\}, \quad \left\{u_\phi^e\right\} = \left[N_\phi\right]\left\{d_\phi\right\}, \quad (11)$$

where

$$\left\{u_u^e\right\} = \left\{u_1, u_2, w, \phi_1, \phi_2, \bar{u}_1^j, \bar{u}_2^j, \overline{w}^j\right\}^T,$$
$$\left\{d_u\right\} = \left\{\ldots, u_{1i}, u_{2i}, w_i, w_{,xi}, w_{,yi}, \phi_{1i}, \phi_{2i}, \bar{u}_{1i}^j, \bar{u}_{2i}^j, \overline{w}_i^j, \times \overline{w}_{,xi}^j, \overline{w}_{,yi}^j, \ldots\right\}^T,$$
$$\left\{u_\phi^e\right\} = \left\{\phi_0^j, E_z^j\right\}^T, \quad \left\{d_\phi\right\} = \left\{\ldots, \phi_{0i}^j, E_{zi}^j, \ldots\right\}^T,$$
$$\left[N_u\right] = \begin{bmatrix} N_i & 0 & 0 & 0 & 0 & 0 \\ 0 & N_i & 0 & 0 & 0 & 0 \\ 0 & 0 & H_i & H_{xi} & H_{yi} & 0 \\ \ldots\ 0 & 0 & 0 & 0 & 0 & N_i \\ 0 & 0 & 0 & 0 & 0 & 0 \\ 0 & 0 & 0 & 0 & 0 & 0 \\ 0 & 0 & 0 & 0 & 0 & 0 \\ 0 & 0 & 0 & 0 & 0 & 0 \end{bmatrix}$$
$$\begin{bmatrix} 0 & \bar{0} & \bar{0} & \bar{0} & \bar{0} & \bar{0} \\ 0 & \bar{0} & \bar{0} & \bar{0} & \bar{0} & \bar{0} \\ 0 & \bar{0} & \bar{0} & \bar{0} & \bar{0} & \bar{0} \\ 0 & \bar{0} & \bar{0} & \bar{0} & \bar{0} & \bar{0} \\ N_i & \bar{0} & \bar{0} & \bar{0} & \bar{0} & \bar{0} \ \cdots \\ 0 & \overline{N_i} & \bar{0} & \bar{0} & \bar{0} & \bar{0} \\ 0 & \bar{0} & \overline{N_i} & \bar{0} & \bar{0} & \bar{0} \\ 0 & \bar{0} & \bar{0} & \overline{H_i} & \overline{H_{xi}} & \overline{H_{yi}} \end{bmatrix},$$

$$\left[N_\phi\right] = \begin{bmatrix} \cdots & N_i & 0 & \cdots \\ & 0 & N_i & \end{bmatrix}. \quad (12)$$

The displacement components, strain components and electric potential can be written in the matrix form in terms of the structural and electrical unknowns. They can be further represented by the interpolation functions and nodal values. Thus, by these processes, the following matrix relations are obtained

$$\begin{aligned} \{U\} &= \left[L_u\right]\left\{u_u^e\right\} = \left[L_u\right]\left[N_u\right]\left\{d_u\right\} = \left[B_u\right]\left\{d_u\right\}, \\ \{\varepsilon\} &= \left[L_\varepsilon\right]\left\{u_u^e\right\} = \left[L_\varepsilon\right]\left[N_u\right]\left\{d_u\right\} = \left[B_\varepsilon\right]\left\{d_u\right\}, \\ \phi^j &= V_b + \left\{L_\phi^j\right\}\left\{u_\phi^j\right\} = V_b + \left\{L_\phi^j\right\}\left[N_\phi\right]\left\{d_\phi^j\right\} \\ &= V_b + \left[B_\phi^j\right]\left\{d_\phi^j\right\}, \\ \left\{E^j\right\} &= -\{F_b\} - \left[L_E^j\right]\left\{u_\phi^j\right\} = -\{F_b\} - \left\{L_E^j\right\} \\ &\quad \times \left[N_\phi\right]\left\{d_\phi^j\right\} = -\{F_b\} - \left[B_E^j\right]\left\{d_\phi^j\right\}, \end{aligned} \quad (13)$$

where

$$\left[B_u\right] = \left[L_u\right]\left[N_u\right], \quad \left[B_\varepsilon\right] = \left[L_\varepsilon\right]\left[N_u\right],$$
$$\left[B_\phi^j\right] = \left\{L_\phi^j\right\}\left[N_\phi\right], \left[B_E^j\right] = \left\{L_E^j\right\}\left[N_\phi\right],$$

$$\left[L_u\right] = \begin{bmatrix} 1 & 0 & C_1^k\frac{\partial}{\partial x} + D_1^k\frac{\partial}{\partial y} & A_1^k & B_1^k \\ 0 & 1 & C_2^k\frac{\partial}{\partial x} + D_2^k\frac{\partial}{\partial y} & A_2^k & B_2^k \\ 0 & 0 & 1 & 0 & 0 \end{bmatrix}$$
$$\begin{bmatrix} H(z-z_k) & \bar{0} & \bar{E}_1^k\frac{\partial}{\partial x} + \bar{F}_1^k\frac{\partial}{\partial y} \\ \bar{0} & H(z-z_k) & \bar{E}_2^k\frac{\partial}{\partial x} + \bar{F}_2^k\frac{\partial}{\partial y} \\ \bar{0} & \bar{0} & H(z-z_k) \end{bmatrix},$$

$$\left[L_s\right] = \begin{bmatrix} \frac{\partial}{\partial x} & 0 & C_1^k\frac{\partial^2}{\partial x^2} + D_1^k\frac{\partial^2}{\partial x\partial y} \\ 0 & \frac{\partial}{\partial y} & C_2^k\frac{\partial^2}{\partial x\partial y} + D_2^k\frac{\partial^2}{\partial y^2} \\ 0 & 0 & C_{2,z}^k\frac{\partial}{\partial x} + \left(1 + D_{2,z}^k\right)\frac{\partial}{\partial y} \\ 0 & 0 & \left(C_{1,z}^k + 1\right)\frac{\partial}{\partial x} + D_{1,z}^k\frac{\partial}{\partial y} \\ \frac{\partial}{\partial y} & \frac{\partial}{\partial x} & C_2^k\frac{\partial^2}{\partial x^2} + \left(C_1^k + D_2^k\right)\frac{\partial^2}{\partial x\partial y} + D_1^k\frac{\partial^2}{\partial y^2} \end{bmatrix}$$

$$\begin{bmatrix}
A_1^k\frac{\partial}{\partial x} & B_1^k\frac{\partial}{\partial x} & H(z-z_j)\frac{\partial}{\partial x} \\
A_2^k\frac{\partial}{\partial y} & B_2^k\frac{\partial}{\partial y} & \bar{0} \\
A_{2,z}^k & B_{2,z}^k & \bar{0} \\
A_{1,z}^k & B_{1,z}^k & \bar{0} \\
A_1^k\frac{\partial}{\partial y}+A_2^k\frac{\partial}{\partial x} & B_1^k\frac{\partial}{\partial y}+B_2^k\frac{\partial}{\partial x} & H(z-z_j)\frac{\partial}{\partial y}
\end{bmatrix}$$

$$\begin{bmatrix}
\bar{0} & \bar{E}_1^k\frac{\partial^2}{\partial x^2}+\bar{F}_1^k\frac{\partial^2}{\partial x\partial y} \\
H(z-z_j)\frac{\partial}{\partial y} & \bar{E}_2^k\frac{\partial^2}{\partial x\partial y}+\bar{F}_2^k\frac{\partial^2}{\partial y^2} \\
\bar{0} & \bar{E}_{2,z}^k\frac{\partial}{\partial x}\left(\bar{F}_{2,z}^k+H(z-z_j)\right)\frac{\partial}{\partial y} \\
\bar{0} & \left[\bar{E}_{1,z}^k+H(z-z_j)\right]\frac{\partial}{\partial x}+\bar{E}_{1,z}^k\frac{\partial}{\partial y} \\
H(z-z_j)\frac{\partial}{\partial x} & \bar{E}_2^k\frac{\partial^2}{\partial x^2}+\left(\bar{E}_1^k+\bar{F}_2^k\right)\frac{\partial^2}{\partial x\partial y}+\bar{F}_1^k\frac{\partial^2}{\partial y^2}
\end{bmatrix},$$

$$\left\{L_\phi^j\right\}=\begin{bmatrix}1-4\frac{\left(z-z_0^j\right)^2}{\left(h^j\right)^2}-\left(z-z_0^j\right)+4\frac{\left(z-z_0^j\right)^3}{\left(h^j\right)^2}\end{bmatrix},$$

$$\left[L_E^j\right]=\begin{bmatrix}
\left(1-4\frac{\left(z-z_0^j\right)^2}{\left(h^j\right)^2}\right)\frac{\partial}{\partial x} & \left(4\frac{\left(z-z_0^j\right)^3}{\left(h^j\right)^2}-\left(z-z_0^j\right)\right)\frac{\partial}{\partial x} \\
\left(1-4\frac{\left(z-z_0^j\right)^2}{\left(h^j\right)^2}\right)\frac{\partial}{\partial y} & \left(4\frac{\left(z-z_0^j\right)^3}{\left(h^j\right)^2}-\left(z-z_0^j\right)\right)\frac{\partial}{\partial y} \\
-8\frac{\left(z-z_0^j\right)}{\left(h^j\right)^2} & 12\frac{\left(z-z_0^j\right)^2}{\left(h^j\right)^2}-1
\end{bmatrix},$$

$$V_b=4\overline{\phi}^j\frac{\left(z-z_0^j\right)^3}{\left(h^j\right)^3},$$

$$\left\{F_b\right\}=\begin{bmatrix}0 & 0 & 12\overline{\phi}^j\frac{\left(z-z_0^j\right)^2}{\left(h^j\right)^3}\end{bmatrix}^T. \tag{14}$$

The governing equations are obtained by using the extended Hamilton principle defined in equation (2). The energy conservation law is applied for a system with piezoelectric materials. Integration by parts and using the variational principle result in the following governing equations

$$\begin{aligned}
\delta\pi_u &= \int_{t_0}^{t}\left[\int_v\left(\rho\ddot{u}_i\delta u_i+\sigma_{ij}\delta\varepsilon_{ij}\right)\mathrm{d}V-\int_S f_i\delta u_i\mathrm{d}S\right]\mathrm{d}t=0,\\
\delta\pi_\phi &= \int_{t_0}^{t}\left[\int_v D_i\delta\phi_{,i}\mathrm{d}V-\int_S q_e\delta\phi\mathrm{d}S\right]\mathrm{d}t=0,
\end{aligned} \tag{15}$$

where $\delta\pi_u$ and $\delta\pi_\phi$ denote the energy functionals of the mechanical and electrical fields, respectively.

Substituting the strain, stress and electric displacement components into the above equation, the elemental equations of motion are obtained and written in matrix form as follows

$$\begin{bmatrix}M_{uu} & 0\\ 0 & 0\end{bmatrix}\begin{Bmatrix}\ddot{d}_u\\ \ddot{d}_\phi\end{Bmatrix}+\begin{bmatrix}C_{uu} & 0\\ 0 & 0\end{bmatrix}\begin{Bmatrix}\dot{d}_u\\ \dot{d}_\phi\end{Bmatrix}+\begin{bmatrix}K_{uu} & K_{u\phi}\\ K_{\phi u} & K_{\phi\phi}\end{bmatrix}\begin{Bmatrix}d_u\\ d_\phi\end{Bmatrix}=\begin{bmatrix}F_u\\ F_\phi\end{bmatrix}, \tag{16}$$

where M_{uu}, C_{uu} and K_{uu} are the element mass, damping and stiffness matrices, respectively, $K_{\phi\phi}$ is the dielectric stiffness matrix, and $K_{u\phi}$ and $K_{\phi u}$ are the stiffness matrices due to the electro-mechanical coupling effect. The electro-mechanical coupling effect causes piezoelectric materials to produce mechanical actuation under input voltages or electrical signals under mechanical deformations. The nodal displacement and nodal electrical variables of the element are denoted by d_u and d_ϕ, respectively. The vectors F_u and F_ϕ are the force vectors corresponding to the applied mechanical and electrical forces, respectively. The detail formulations of these matrices are shown below.

$$\begin{aligned}
M_{uu}^e &= \int_V B_u^T\rho B_u\mathrm{d}V,\\
K_{uu}^e &= \int_V B_\varepsilon^T Q B_\varepsilon\mathrm{d}V,\\
K_{\phi\phi}^e &= \int_V B_E^T b B_E\mathrm{d}V,\\
K_{u\phi}^e &= \int_V B_\varepsilon^T\mathrm{d}B_E\mathrm{d}V=-K_{\phi u}^{e^T},\\
F_u^e &= \int_s B_u^T f\mathrm{d}S+\int_V B_u^T F_b\mathrm{d}V,\\
F_\phi^e &= -\int_s B_\phi^T q_e\mathrm{d}S-\int_V B_E^T b F_b\mathrm{d}V.
\end{aligned} \tag{17}$$

For the damping matrix, we prefer using the proportional viscous damping which is the simplest damping case and can be easily implemented in linear vibration analysis

$$C_{uu}=\alpha M_{uu}+\beta K_{uu}. \tag{18}$$

The governing equation in matrix form is modified by applying the matrix condensation, so that it takes on the following form

$$M_{uu}\ddot{d}_u+C_{uu}\dot{d}_u+Kd_u=F, \tag{19}$$

Table 1. Material properties of host composite laminae and PZT-5H.

Material properties	Host laminae	PZT-5H
Young's modulus (GPa)	$E_1 = 372$	$E = 62$
	$E_2 = E_3 = 4.12$	
Shear modulus (GPa)	$G_{12} = G_{13} = 3.99$	$G = 23.67$
	$G_{23} = 3.6$	
Poisson ratio	$\nu_{12} = \nu_{13} = 0.275$	$\nu = 0.31$
	$\nu_{23} = 0.42$	
Density ρ (kg m^{-3})	1788.5	7500
Piezoelectric constant (m V^{-1})	—	$d_{31} = d_{32} = -274 \times 10^{-12}$
		$d_{24} = d_{15} = 741 \times 10^{-12}$
Permittivity (nF m^{-1})	—	$b_{11} = b_{22} = b_{33} = 14.41$
Length (m)	0.3	0.05
Width (m)	0.06	0.04
Thickness (m)	0.125×10^{-3}	0.25×10^{-3}

where the general forms of the stiffness matrix and force vector have the following expressions

$$K = K_{uu} - K_{u\phi}K_{\phi\phi}^{-1}K_{\phi u}, \quad F = F_u - K_{u\phi}K_{\phi\phi}^{-1}F_{\phi}. \tag{20}$$

3. Numerical results and discussion

In this subsection, the numerical results are investigated using a 16 layer cross-ply ($[0/90]_{4s}$) laminate with surface bonded piezoelectric actuator and sensor. The material properties of a single lamina and piezoelectric material (PZT-5H) are given in table 1. The finite element mesh consists of 60 by 12 elements in the length and width directions, respectively, which is fine enough to obtain an accurate system response. The actuator is preset to be partially debonded, considering two debonding cases, viz. edge and inner debonding, as shown in figure 3. The debonding area varies from 10 to 50% in the edge debonding case and 20 to 60% in the inner debonding case. Subsequently, the dynamic behaviors of the smart composite laminate with partially debonded piezoelectric actuator are investigated and the effects of debonding on the dynamic characteristics are presented in the following subsections.

3.1. Frequency response

The debonding failure of a piezoelectric actuator obviously affects the stiffness of the structure as well as its natural frequencies [29]. This is discussed in many existing works on structural health monitoring [15, 26, 27]. Thus, it is necessary to investigate the effect of the debonding of the actuator on its dynamic characteristics by frequency response analysis. To efficiently obtain the frequency response of a plate excited by an electric harmonic load with a magnitude of 1 V, the general mode superposition method can be adopted. The proportional damping ratios α and β are both chosen to be 0.000 01. Firstly, the eigenvalues and eigenvectors are calculated from the free vibration analysis and, then, the normalized eigenvectors are used to conduct the modal transformation from global coordinates to modal coordinates by the following relation

$$\{d_u\} = [\Phi]\{\eta\}, \tag{21}$$

where $[\Phi]$ is the ordered and normalized eigenvector matrix and $\{\eta\}$ is the modal coordinate vector.

Substituting equation (21) into (19) and left multiplying $[\Phi]^T$, the governing equation is diagonalized and each mode is decoupled. The ith modal equation is as follows:

$$\ddot{\eta}_i + 2\xi_i\omega_i\dot{\eta}_i + \omega_i^2\eta_i = \left|\bar{f}_i\right|\cos(\omega t). \tag{22}$$

Thus, the frequency response of each mode can be calculated by solving the second order differential equation, separately. Using the mode superposition method, the frequency responses of the global displacements are obtained. The sensor output is obtained by the coupling effect, the second row of equation (16).

The frequency response curves of the tip center displacement and sensor output are shown in figures 4 and 5, respectively, in the case of the edge debonded actuator. The magnitudes of the frequency responses are all expressed in decibels (dB), that is $20 \times \log_{10}\left(\left|A_1\right|/\left|A_2\right|\right)$. The quantity A_1 is the amplitude of the frequency response, and A_2 represents the reference amplitude of a displacement or sensor output such as 1 m or 1 V, respectively. It is found that the effect of actuator debonding on the natural frequencies is difficult to observe from the frequency analysis. For this kind of structure, even with 50% debonding, the shift of the natural frequencies is still not significant. Figure 6 shows the effect of actuator debonding on the first five natural bending frequencies. It is apparent that with increasing debonding area, the five natural bending frequencies decrease. However, the amount of frequency reduction is within 1% for all five natural frequencies. On the other hand, it is found that the actuator debonding affects the magnitude of the frequency response. From the frequency response graphs, it is found that as the debonding area increases, the magnitude of the frequency response greatly decreases. This is due to the fact that the debonding of the actuator causes a reduction of the bonding area between the actuator and the host plate. Since the actuation force is transferred through the contacted interface, decreasing the bonding area causes a reduction of the force transfer capability. Thus, if the transferred actuation force is decreased, the system response is attenuated in consequence.

The frequency response in the inner debonding case is investigated as well, and the results are presented in figures 7 and 8. The results lead to similar conclusions to the edge debonding case in that the natural frequency shift is not easy to identify. Figure 9 compares the natural frequency change due to the inner debonding effect. The change is also within 1% for all five natural bending frequencies. However, it should be noted that the reduction in magnitude of the frequency response is not as much as that in the edge debonding case. This demonstrates that the force transfer capability from the actuator to the host plate in the inner debonding case is better than that in the edge debonding case. Unlike the edge

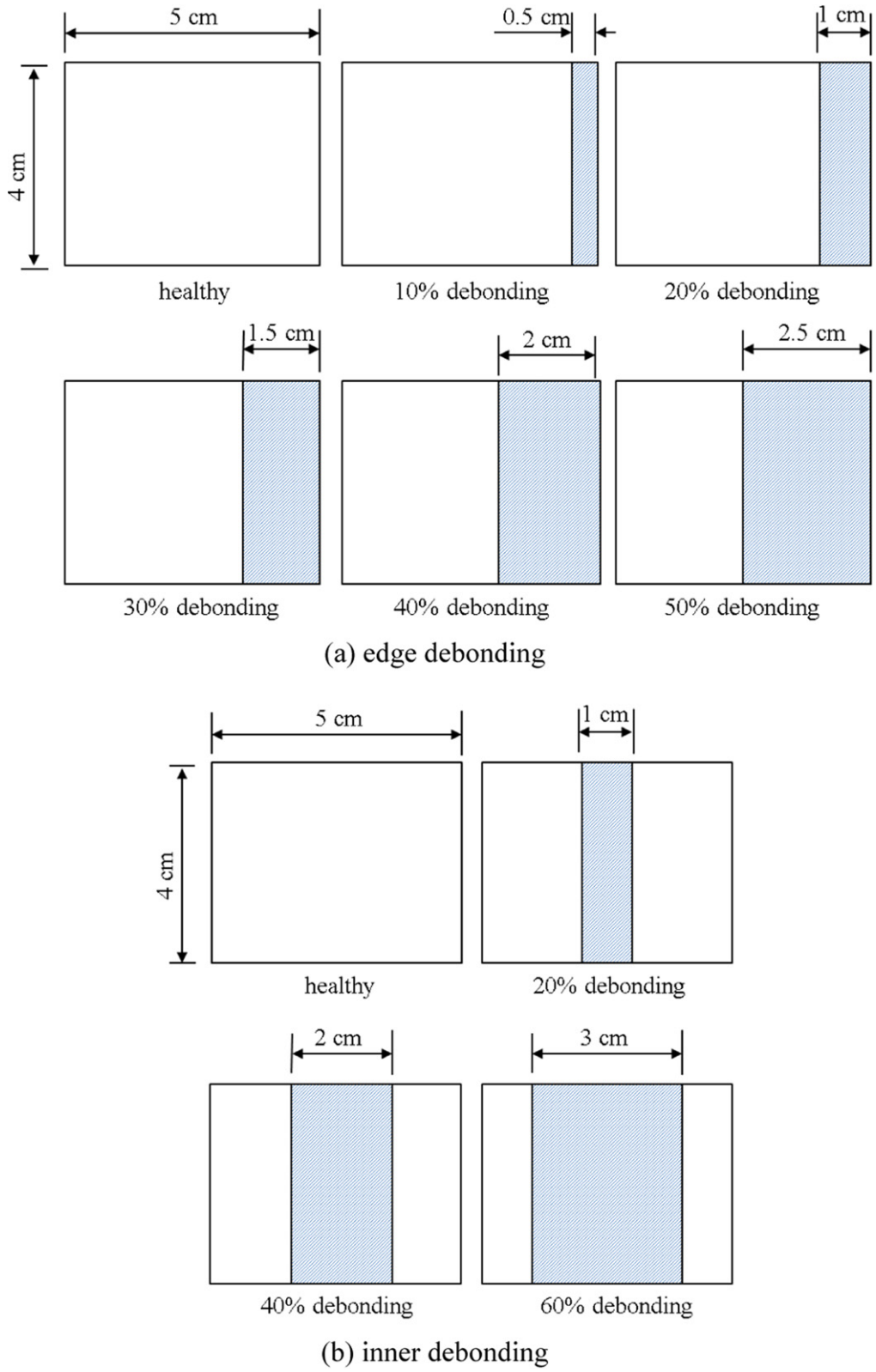

Figure 3. Details of actuator debonding sizes and locations, (a) edge debonding, (b) inner debonding.

debonding case, the debonded piezoelectric actuator in the inner debonding case can generate an actuating force due to the presence of a bonding area on both sides. Although it has a 60% debonding area, the reduction of the magnitude is very small. Thus, from the frequency response results, it can be concluded that the effect of the inner debonding of the actuator on its actuation ability is much smaller than that in the edge debonding case.

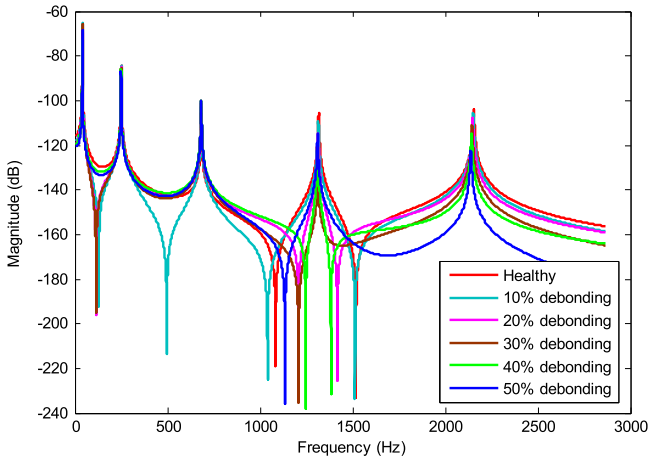

Figure 4. Frequency responses of the tip displacement in the healthy laminate and edge debonded actuator cases.

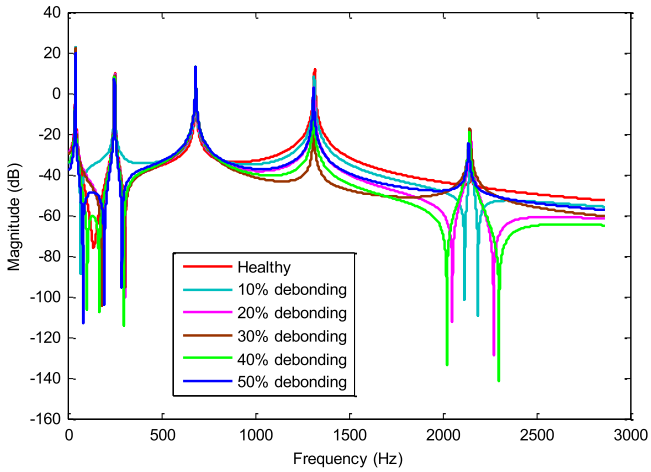

Figure 5. Frequency responses of the sensor output in the healthy laminate and edge debonded actuator cases.

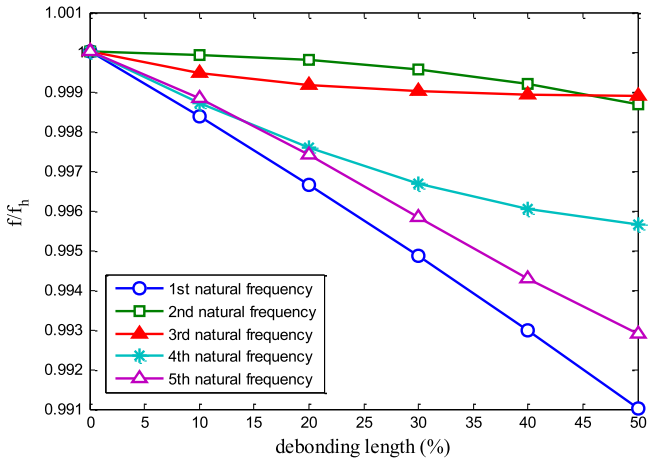

Figure 6. Effects of the actuator debonding on the first five bending natural frequencies for the edge debonding actuator.

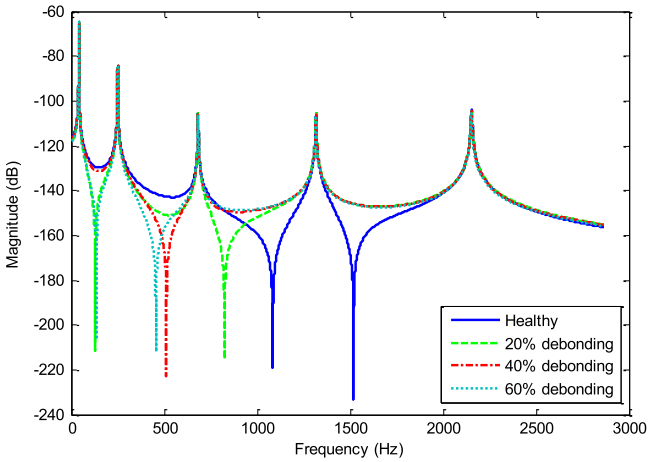

Figure 7. Frequency responses of the tip displacement in the healthy laminate and inner debonded actuator cases.

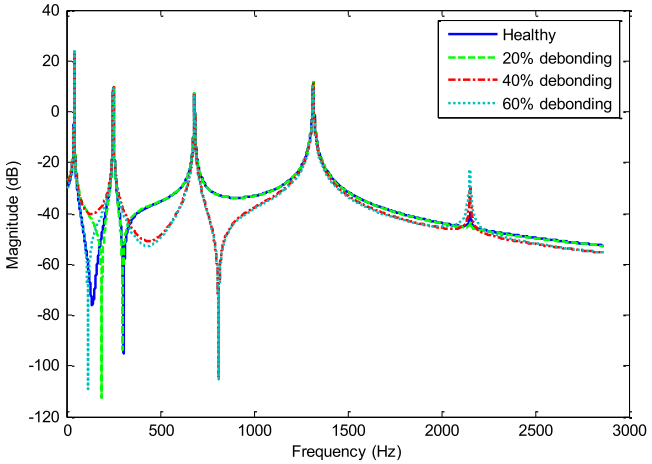

Figure 8. Frequency responses of the sensor output in the healthy laminate and inner debonded actuator cases.

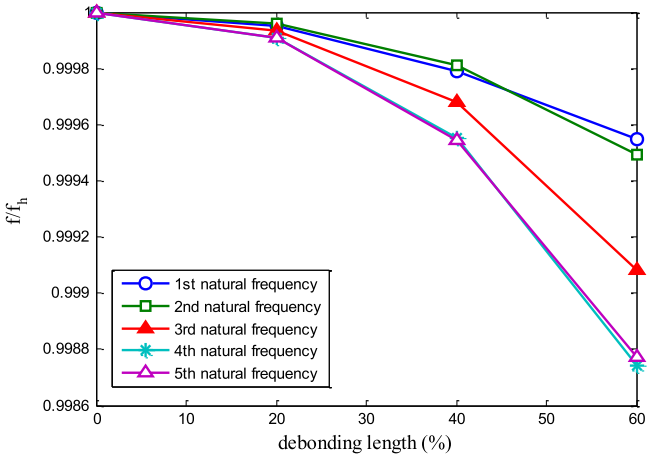

Figure 9. Effects of the actuator debonding on the first five bending natural frequencies for the inner debonding actuator.

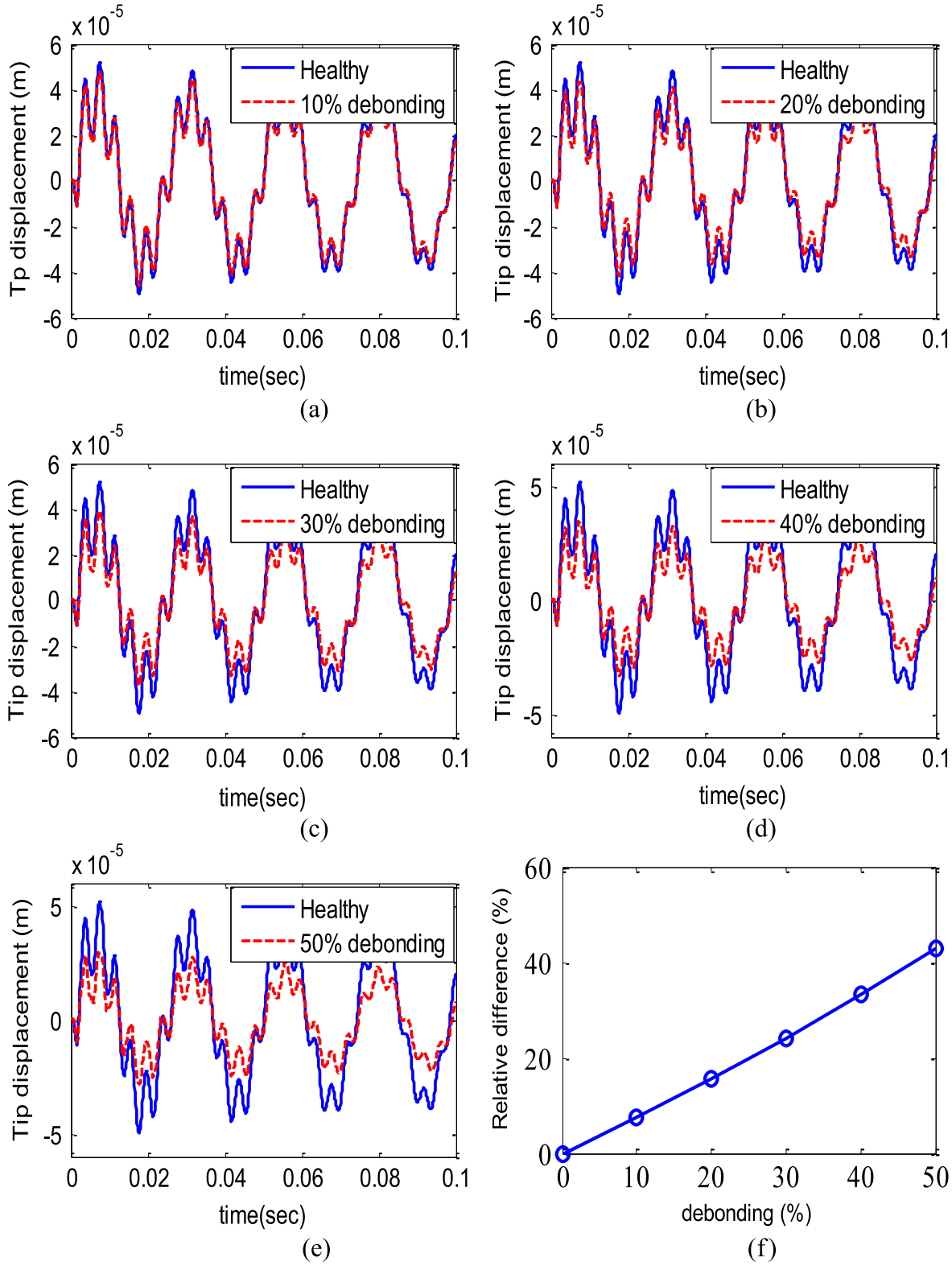

Figure 10. Transient responses of the tip displacement under the electrical impulse load in the healthy laminate and edge debonded actuator cases, (a) 10%, (b) 20%, (c) 30%, (d) 40%, (e) 50%, (f) relative difference of the peak values.

3.2. Transient response

In the previous section, we found that the debonding causes a reduction of the actuation force transfer capability. This effect also influences the system response in the time domain as well. Thus, we also investigated the transient responses of the smart composite laminate with partially debonded piezoelectric actuator. The clamped plate is excited by a 100 V electric impulse load for a time period of 10 ms and the tip

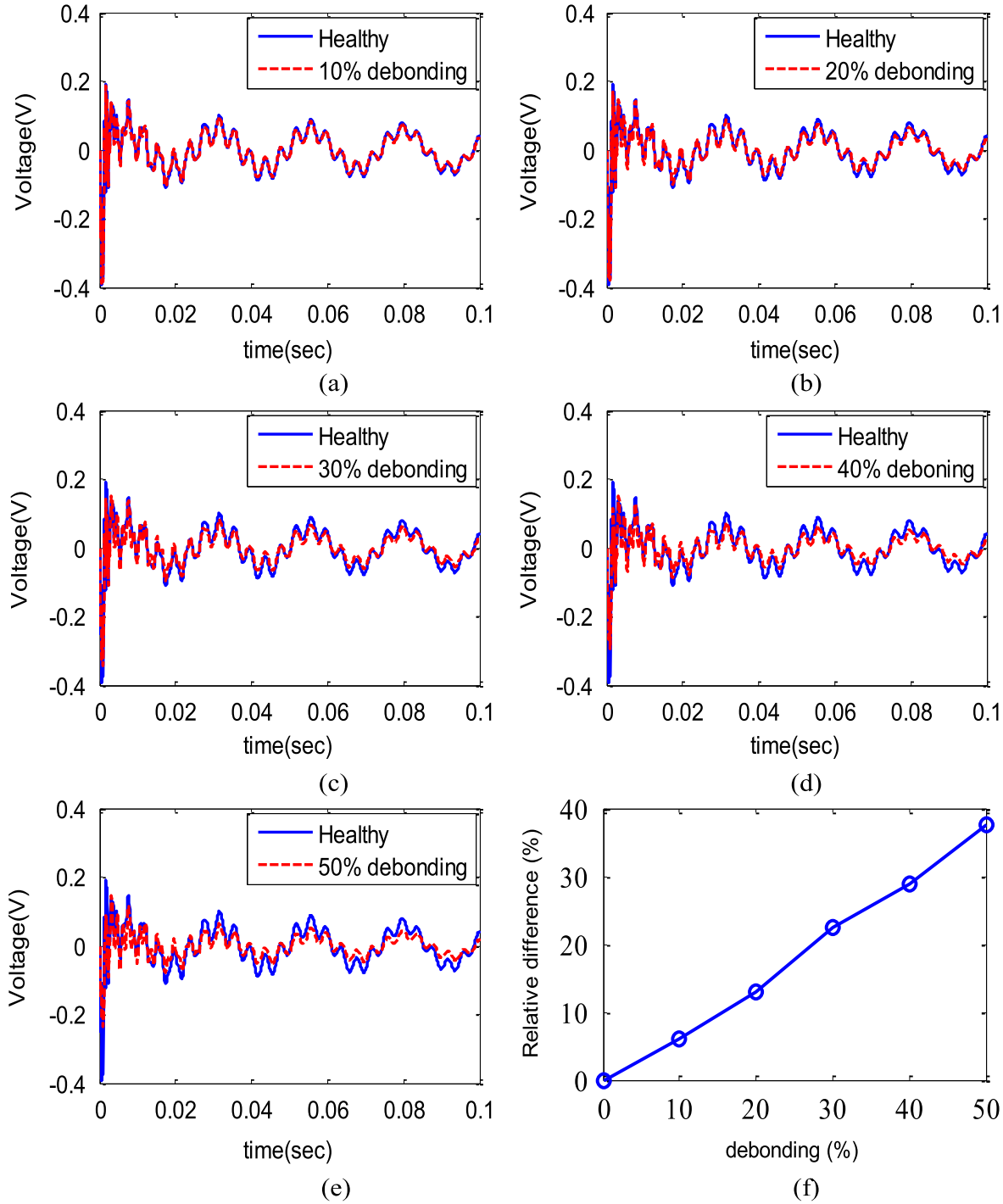

Figure 11. Transient responses of the sensor output under the electrical impulse load in the healthy laminate and edge debonded actuator cases, (a) 10%, (b) 20%, (c) 30%, (d) 40%, (e) 50%, (f) relative difference of the peak values.

displacement and sensor output are calculated as the system response. For the finite element method based governing equation, the transient response can be solved by the direct time integration method. In the current linear vibration problem, we prefer using the Newmark time integration, which is conventionally used to solve finite element method based linear vibration problems. In the algorithm, the displacement variable and its first derivative are approximated by Taylor's expansions with terms up to the second derivative. With the help of these Taylor's expansions, the governing equation can be reduced to set of algebraic equations. The governing equation can be solved through an iterative process involving only the given initial conditions and the force input for each time step. The transient responses of the tip displacement in the edge debonding cases are shown in figures 10(a)–(f). It is found that a difference in the peak values between the healthy and debonded laminates clearly appears in each graph. The 10% debonding case shows the smallest relative difference

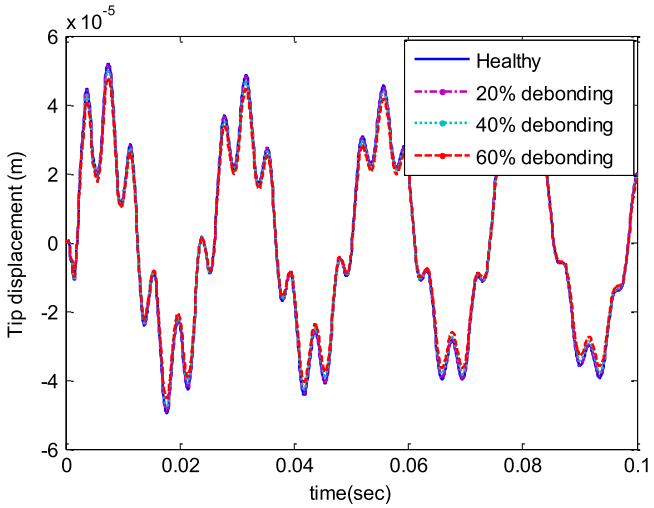

Figure 12. Transient response of the tip displacement under the electrical impulse load in the healthy laminate and inner debonded actuator cases.

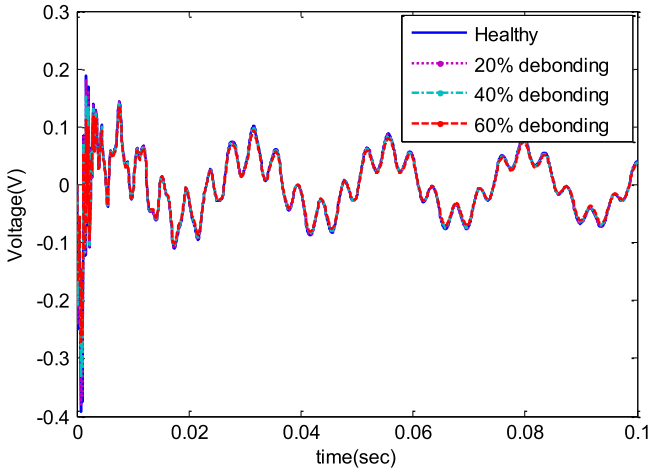

Figure 13. Transient response of the sensor output under the electrical impulse load in the healthy laminate and inner debonded actuator cases.

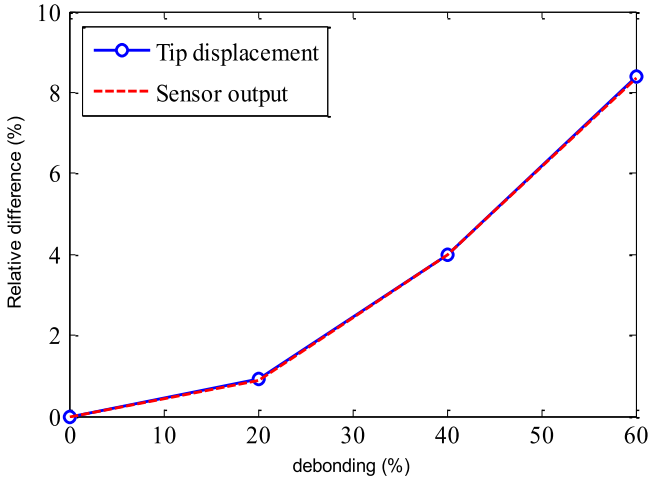

Figure 14. Relative difference of the peak values for the tip displacement and sensor output under the electrical impulse load in the healthy laminate and inner debonded actuator cases.

and the 50% debonding case shows the largest one. The relative difference of the peak value is defined by the following equation

$$\text{Relative} = \left(\text{Peak}_{\text{healthy}} - \text{Peak}_{\text{debonding}}\right)/ \times \text{Peak}_{\text{healthy}} \times 100\%. \quad (23)$$

The effect of the debonding area on the relative difference in the peak values is shown in figure 10(f). From the curve, it is found that with increasing debonding area, the relative difference increases almost linearly. The 50% debonding of the actuator causes an almost 50% drop in the peak value of the displacement output. The results of the tip displacement output also show that the actuation ability decreases considerably due to the actuator debonding effect for such an edge debonded actuator. On the other hand, the sensor outputs are also calculated and shown in figures 11(a)–(f). Since the sensor output is dependent on the mechanical strain, the attenuation of the vibration definitely leads to a reduction of the induced strain. Thus, the actuator debonding affects the vibration amplitude and consequently decreases the sensor output. The results provided good evidence of this phenomenon. Figures 11(a)–(f) well illustrate the reduction in the sensor output due to the actuator debonding effect. The percentage relative difference in the peak value also increases almost linearly with increasing debonding area. Thus, using these transient response results, the actuation ability of the actuator can be well evaluated.

In the actuator inner debonding case, the transient responses are also investigated and the results are shown in figures 12–14. From the previous frequency response analysis, we already know that the reduction in actuation ability in the inner debonding case is less than that in the edge deboning case. This conclusion is confirmed by the transient response results. The transient responses of the tip displacement and sensor output are shown in figures 12 and 13, respectively. It is found that the differences in the peak value are very small in the 20, 40 and even 60% debonding cases. The relative differences in the peak values for the tip displacement and sensor output are shown in figure 14. Since the sensor outputs are induced by the mechanical strain, the relative differences of peak values are same for both the tip displacement and sensor output. From the graph, it can be seen that although the actuator suffers from 60% debonding, the relative difference in the peak value is still less than 10% for both the tip displacement and sensor output. This result is very different from that of the edge debonding case. However, the transient response results are in good agreement with the frequency response results. It can be concluded that the effect of inner debonding of the actuator on the structural response is much smaller than that of edge debonding.

4. Concluding remarks

In this work, the modeling of a smart composite laminate with partially debonded piezoelectric actuator was developed. Using the developed modeling, the dynamic characteristics

were examined in both the frequency and time domains. The actuators suffering from both edge debonding and inner debonding were investigated for the analysis of the reduction in their actuation ability. The numerical results demonstrated that the reduction in actuation ability in the edge debonding case is much larger than that in the inner debonding case. Based on these dynamic analysis results, it is concluded that the actuator debonding failures, especially the edge debonding, have great effect on the actuation ability and reduce the controllability in active structures. Since the actuator debonding failure may happen during their service life, it is necessary to take the debonding failure into the consideration as an uncertainty parameter to make the system damage tolerable. We believe that the proposed method well describes the effect of actuator debonding on the dynamic behaviors of such laminated smart composite structures. The proposed modeling could be used to analyze the actuator debonding failures in engineering applications.

Acknowledgments

This work was supported by the Center for Advanced Meta-Materials (CAMM) funded by the Ministry of Science, ICT and Future Planning as Global Frontier Project (CAMM-2014M3A6B3063711). This work was also supported by the Basic Science Research Program of the National Research Foundation of Korea (NRF), funded by the Ministry of Education (NRF-2014R1A1A2A10054019).

References

[1] Chopra I 2002 Review of state of art of smart structures and integrated systems *AIAA J.* **40** 2145–87
[2] Franco Correia V M, Aguiar Gomes M A, Suleman A, Mota Soares C M and Mota Soares C A 2000 Modeling and design of adaptive composite structures *Comput. Method Appl. Mech.* **185** 325–46
[3] Chandrashekhara K and Agarwal A N 1993 Active vibration control of laminated composite plates using piezoelectric devices: a finite element approach *J. Intel. Mater. Syst. Struct.* **4** 496–508
[4] Kim H S, Kim J H and Kim J 2011 A review of piezoelectric energy harvesting based on vibration *Int. J. Precis. Eng. Man.* **12** 1129–41
[5] Lee S and Youn B D 2011 A new piezoelectric energy harvesting design concept: multimodal energy harvesting skin *IEEE Trans. Ultrason. Ferroelectr. Freq. Control* **58** 629–45
[6] Izadi M and Tahani M 2010 Analysis of interlaminar stresses in general cross-ply laminates with distributed piezoelectric actuators *Compos. Struct.* **92** 757–68
[7] Mannini A and Gaudenzi P 2004 Multi-layer higher-order finite elements for the analysis of free-edge stresses in piezoelectric actuated laminates *Compos. Struct.* **63** 263–70
[8] Huang B and Kim H S 2014 Free-edge interlaminar stress analysis of piezo-bonded composite laminates under symmetric electric excitation *Int. J. Solids Struct.* **51** 1246–52
[9] Alnefaie K 2009 Finite element modeling of composite plates with internal delamination *Compos. Struct.* **90** 21–7
[10] Pardoen G C 1989 Effect of delamination on the natural frequencies of composite laminates *J. Compos. Mater.* **23** 1200–15
[11] Kapuria S, Kumari P and Nath J K 2010 Efficient modeling of smart piezoelectric composite laminates: a review *Acta Mech.* **214** 31–48
[12] Ghugal Y M and Shimpi R P 2002 A review of refined shear deformation theories of isotropic and anisotropic laminated plates *J. Reinf. Plast. Compos.* **21** 775–813
[13] Seeley C E and Chattopadhyay A 1999 Modeling of adaptive composites including debonding *Int. J. Solids Struct.* **36** 1823–43
[14] Chattopadhyay A, Gu H and Dragomir-Daescu D 1999 Dynamics of delaminated composite plates with piezoelectric actuators *AIAA J.* **37** 248–54
[15] Charles E S and Aditi C 1998 Experimental investigation of composite beams with piezoelectric actuation and debonding *Smart Mater. Struct.* **7** 502
[16] Nanda N and Sahu S K 2012 Free vibration analysis of delaminated composite shells using different shell theories *Int. J. Press. Vessels Pip.* **98** 111–8
[17] Kim H S, Chattopadhyay A and Ghoshal A 2003 Dynamic analysis of composite laminates with multiple delamination using improved layerwise theory *AIAA J.* **41** 1771–9
[18] Ghoshal A, Kim H S, Chattopadhyay A and Prosser W H 2005 Effect of delamination on transient history of smart composite plates *Finite Elem. Anal. Des.* **41** 850–74
[19] Kim H S, Ghoshal A, Chattopadhyay A and Prosser W H 2004 Development of embedded sensor models in composite laminates for structural health monitoring *J. Reinf. Plast. Compos.* **23** 1207–40
[20] Chattopadhyay A, Kim H S and Ghoshal A 2004 Nonlinear vibration analysis of smart composite structures with discrete delamination using a refined layerwise theory *J. Sound Vib.* **273** 387–407
[21] Oh J, Cho M and Kim J S 2005 Dynamic analysis of composite plate with multiple delaminations based on higher-order zigzag theory *Int. J. Solids Struct.* **42** 6122–40
[22] Kim J S and Cho M 2003 Efficient higher order shell theory for laminated composites with multiple delaminations *AIAA J.* **41** 941–50
[23] Ghoshal A, Kim H S, Kim J, Choi S B, Prosser W H and Tai H 2006 Modeling delamination in composite structures by incorporating the Fermi–Dirac distribution function and hybrid damage indicators *Finite Elem. Anal. Des.* **42** 715–25
[24] Kim H S, Ghoshal A, Kim J and Choi S B 2006 Transient analysis of delaminated smart composite structures by incorporating the Fermi–Dirac distribution function *Smart Mater. Struct.* **15** 221–31
[25] Kim H S, Kim J, Choi S B, Ghoshal A and Chattopadhyay A 2007 Modal-strain-based damage index of laminated composite structures using smooth transition of displacements *AIAA J.* **45** 2972–8
[26] Sun D, Tong L and Atluri S N 2001 Effects of piezoelectric sensor/actuator debonding on vibration control of smart beams *Int. J. Solids Struct.* **38** 9033–51
[27] Kumar D N, Raja S and Tadashige I 2007 Active vibration control of smart plates with partially debonded multilayered PZT actuators *Smart Mater. Struct.* **16** 1584
[28] Kim H S, Chattopadhyay A and Ghoshal A 2003 Characterization of delamination effect on composite laminates using a new generalized layerwise approach *Comput. Struct.* **81** 1555–66
[29] Campanelli R W and Engblom J J 1995 The effect of delaminations in graphite/PEEK composite plates on modal dynamic characteristics *Compos. Struct.* **31** 195–202